Supporting Information

Effect of Bromine Doping on Charge Transfer, Ion Migration and Stability of the Single Crystalline $MAPb(Br_xI_{1-x})_3$ Photodetector

Apurba Mahapatra,[a] Daniel Prochowicz,[b,] Joanna Kruszyńska,[b] Soumitra Satapathi,[c] Seckin Akin,[d] Hemant Kumari,[e] Pawan Kumar,[a] Ziba Fazel,[f] Mohammad Mahdi Tavakoli[g,h]* and Pankaj Yadav[e,*]*

[a] Department of Physics & Astronomy, National Institute of Technology, Rourkela, 769008, India,

[b] Institute of Physical Chemistry, Polish Academy of Sciences, Kasprzaka 44/52, 01-224 Warsaw, Poland.

[c] Department of Physics, Indian Institute of Technology Roorkee, Roorkee, Haridwar, Uttarakhand 247667, India.

[d] Department of Metallurgical and Materials Engineering, Karamanoglu Mehmetbey University, 70200 Karaman, Turkey.

[e] Department of Solar Energy, School of Technology, Pandit Deendayal Petroleum University, Gandhinagar-382 007, Gujarat, India.

[f] *Electrical Engineering Department, Sharif University of Technology, Tehran, 11365-11155, Iran*

[g] *Department of Materials Science and Engineering, Sharif University of Technology, 14588 Tehran, Iran*

[h] Department of Electrical Engineering and Computer Science, Massachusetts Institute of Technology, Cambridge, MA 02139, USA.

Corresponding authors: dprochowicz@ichf.edu.pl; pankaj.yadav@sse.pdpu.ac.in; mtavakol@mit.edu

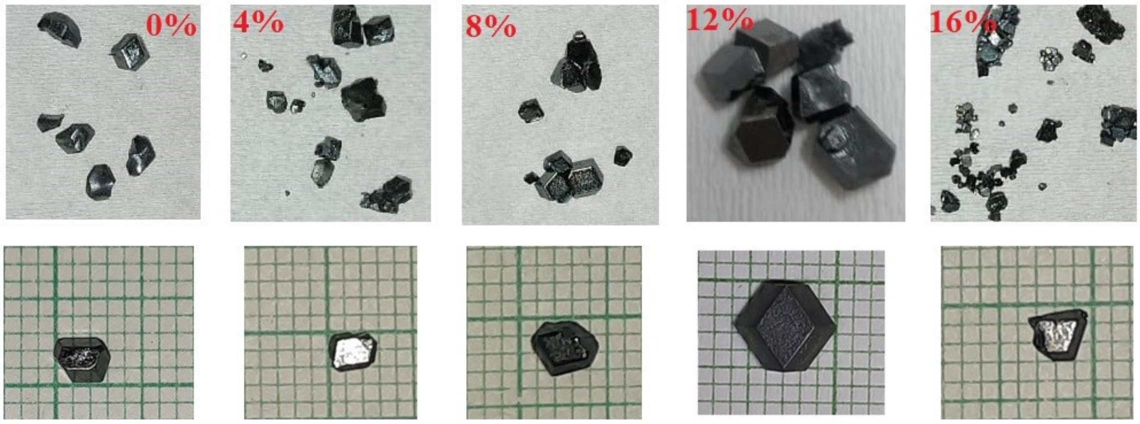

Fig. S1. Photographs of the resulting $MAPb(Br_xI_{1-x})_3$ (x = 0, 0.4, 0.8, 0.12, 0.16) SCs.

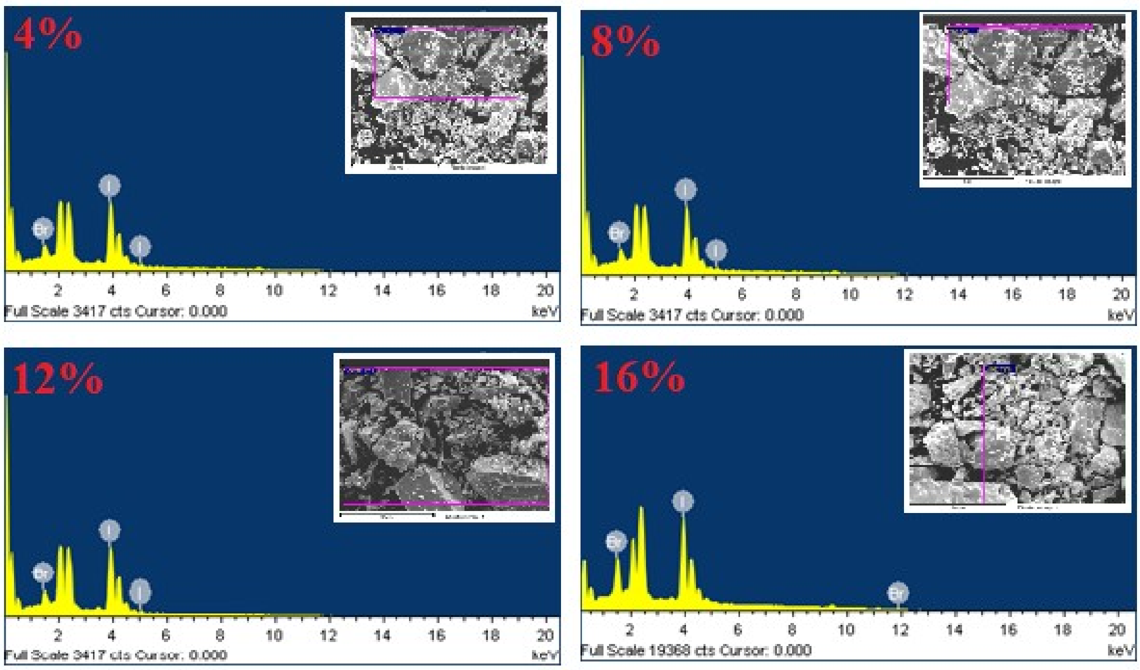

Fig. S2. EDX data for $MAPb(Br_xI_{1-x})_3$ (x = 0.4, 0.8, 0.12, 0.16) SCs grounded powders.

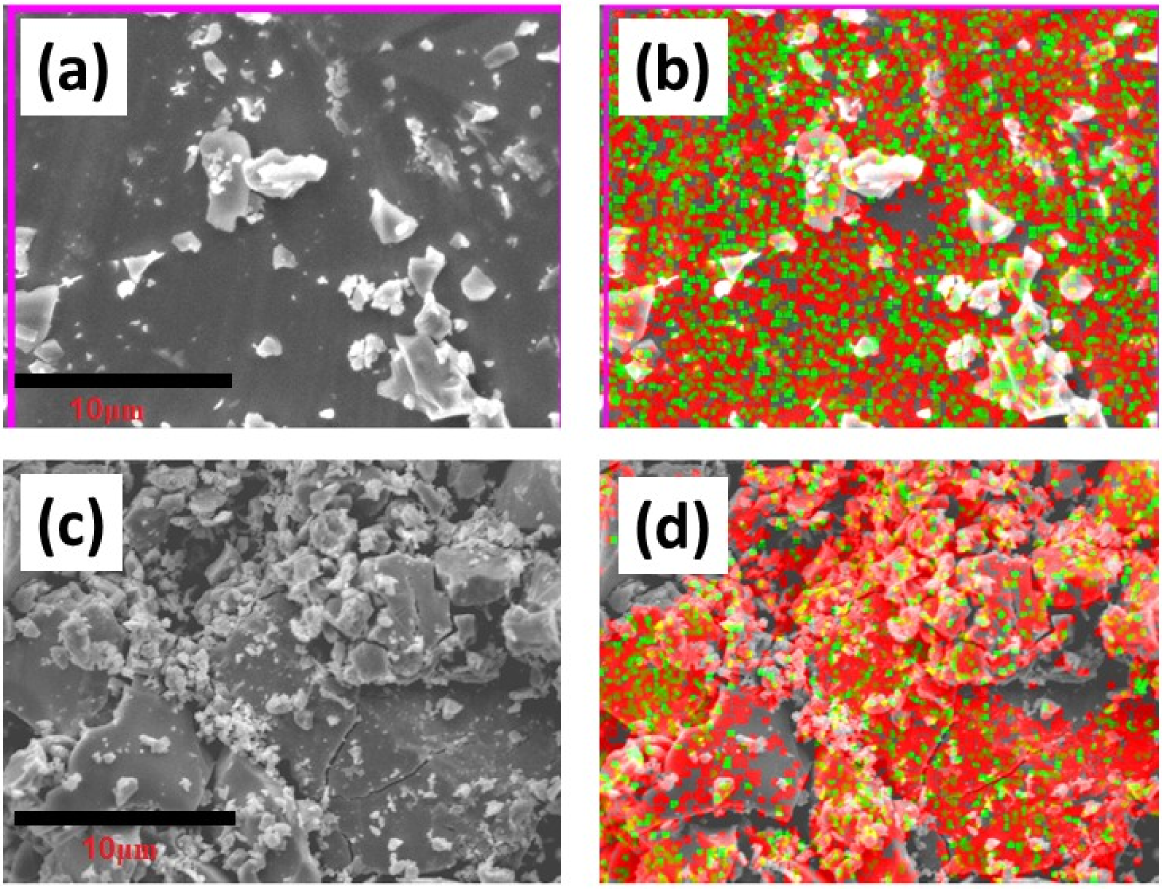

Fig. S3. EDX mapping of Br doped SCs. SEM images of (a) surface (c) crushed to powder. Overall mapping elements on the same spot of (b) surface (d) crushed powder corresponding to iodide (red) and bromide (green). The scale bar is 10 μm.

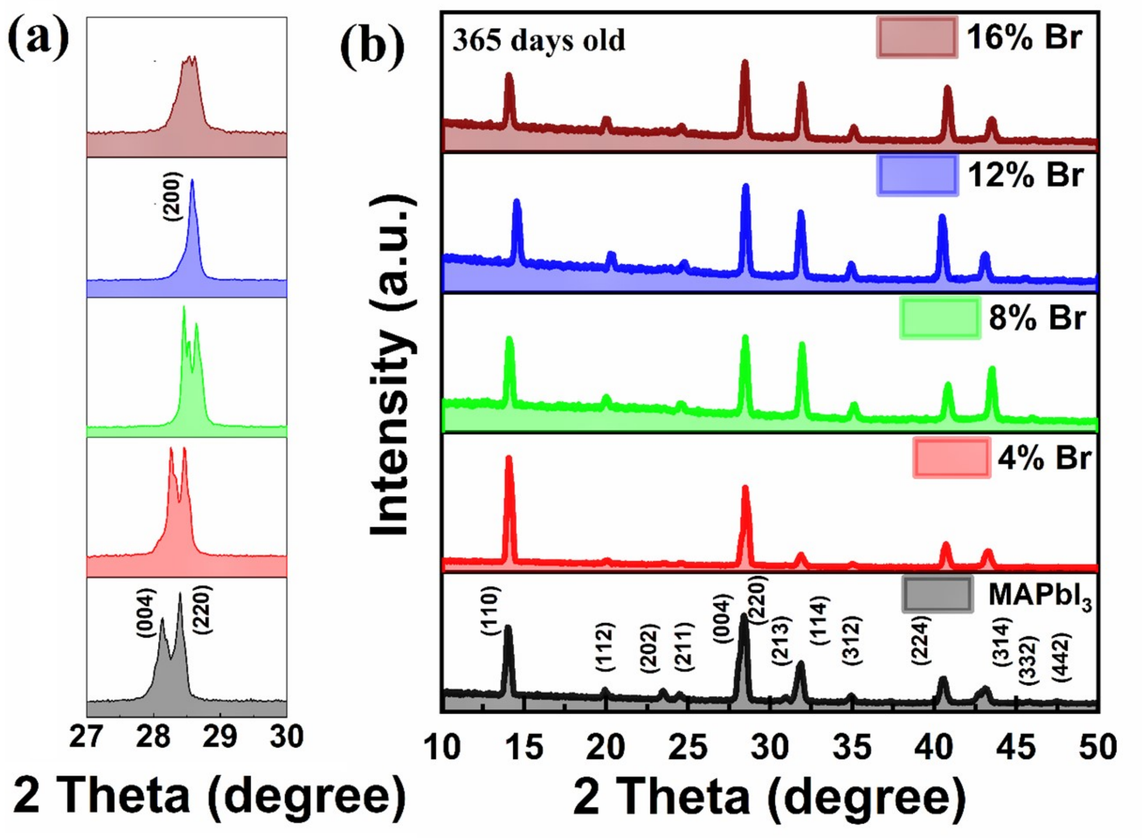

Fig. S4. (a) Enlarged view of the XRD peak at around 28°. (b) XRD patterns of the 365 days aged $MAPbI_3$ and $MAPb(Br_xI_{1-x})_3$ grounded powders.

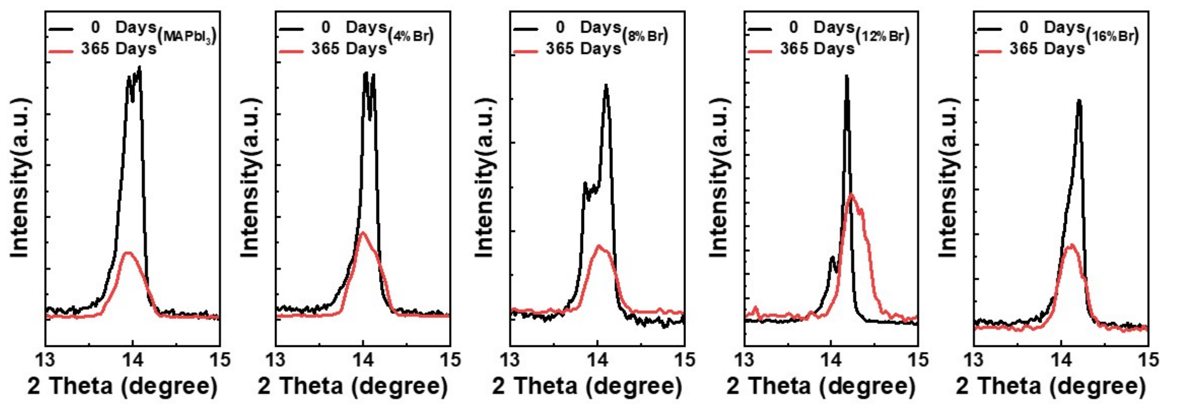

Fig. S5. Intensity comparison of XRD patterns of the fresh and 365 days aged $MAPbI_3$ and $MAPb(Br_xI_{1-x})_3$ SC grounded powders.

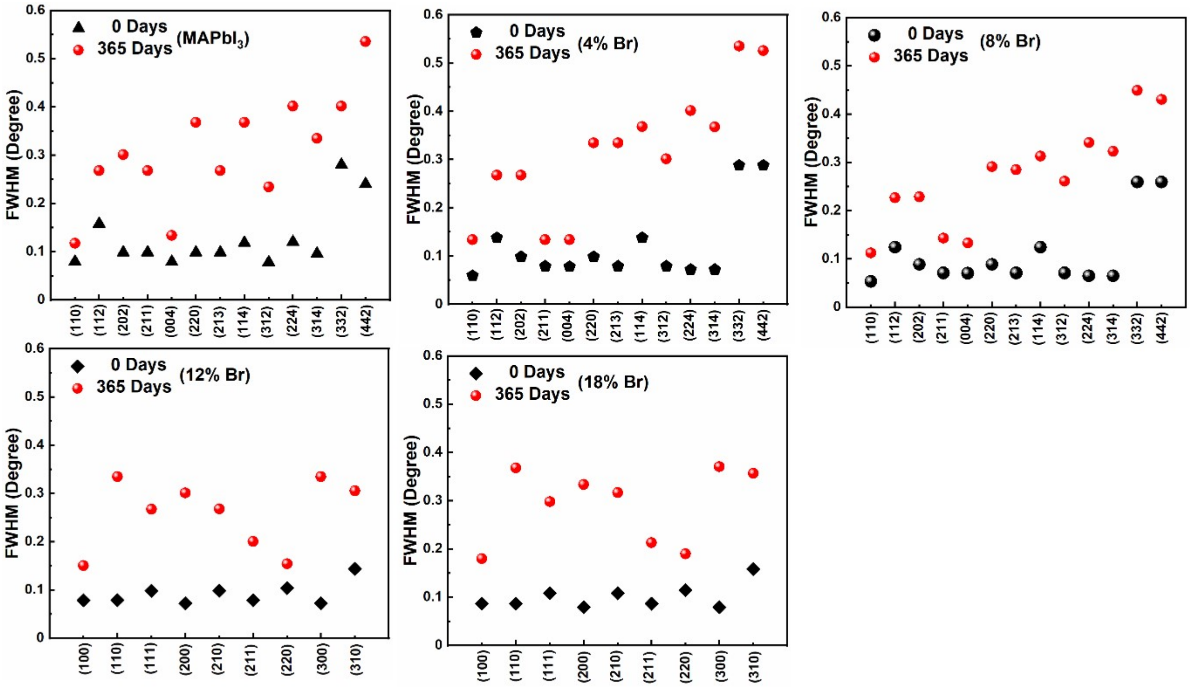

Fig. S6. Analysis of the full width at half maxima (FWHM) for the pXRD peak of fresh and aged $MAPbI_3$ and $MAPb(I_{1-x}Br_x)_3$ grounded powders.

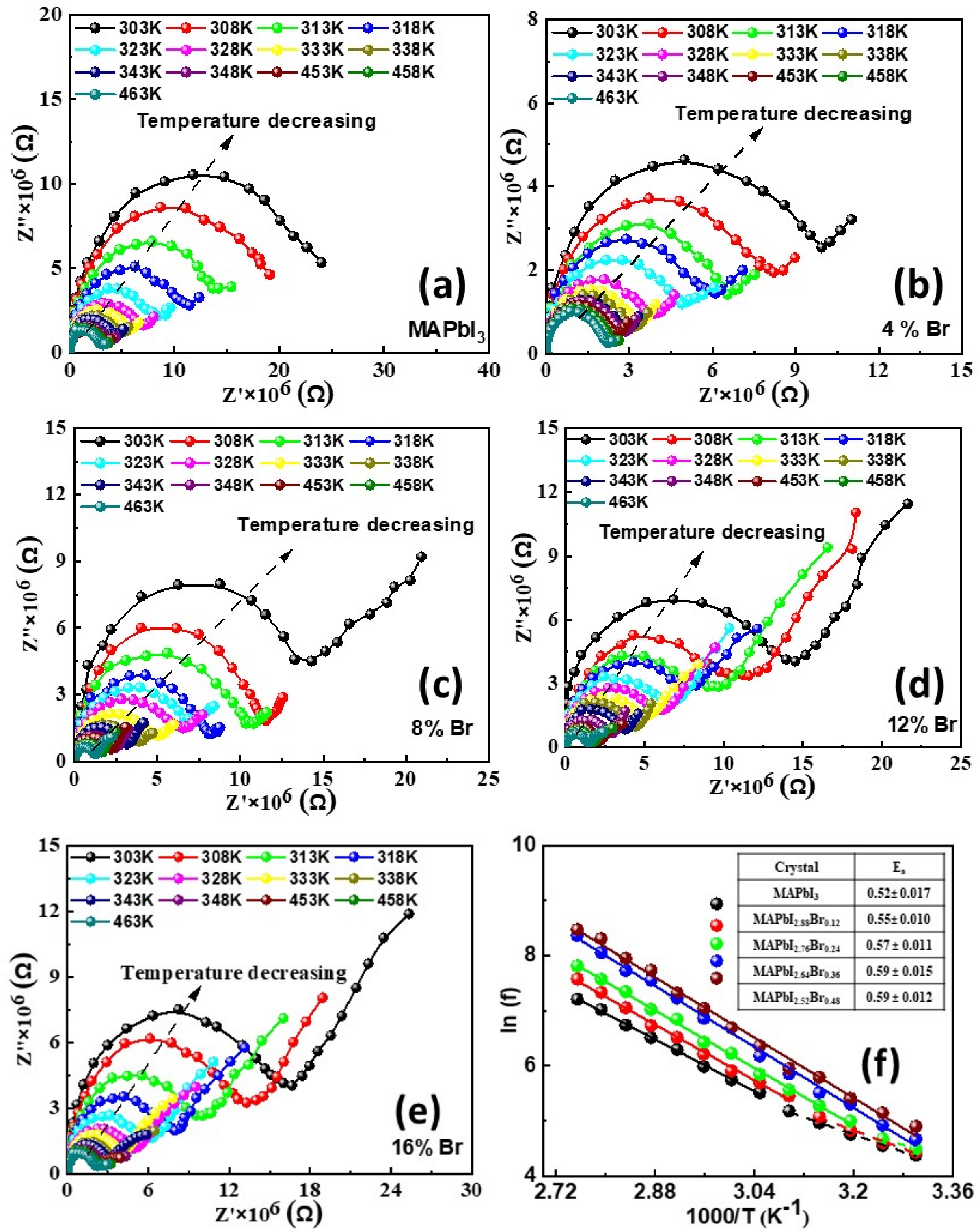

Crystal	E_a
$MAPbI_3$	0.52± 0.017
$MAPbI_{2.88}Br_{0.12}$	0.55± 0.010
$MAPbI_{2.76}Br_{0.24}$	0.57 ± 0.011
$MAPbI_{2.64}Br_{0.36}$	0.59 ± 0.015
$MAPbI_{2.52}Br_{0.48}$	0.59 ± 0.012

Fig. S7. Temperature-dependent EIS data of (a) $MAPbI_3$ and (b-e) $MAPb(Br_xI_{1-x})_3$ SCs in the frequency range of 1MHz to 1Hz. (f) Arrhenius plots of the try to escape frequency (f_0) *vs*. 1000/T of $MAPbI_3$ and $MAPb(Br_xI_{1-x})_3$ SCs (decreasing cycle).

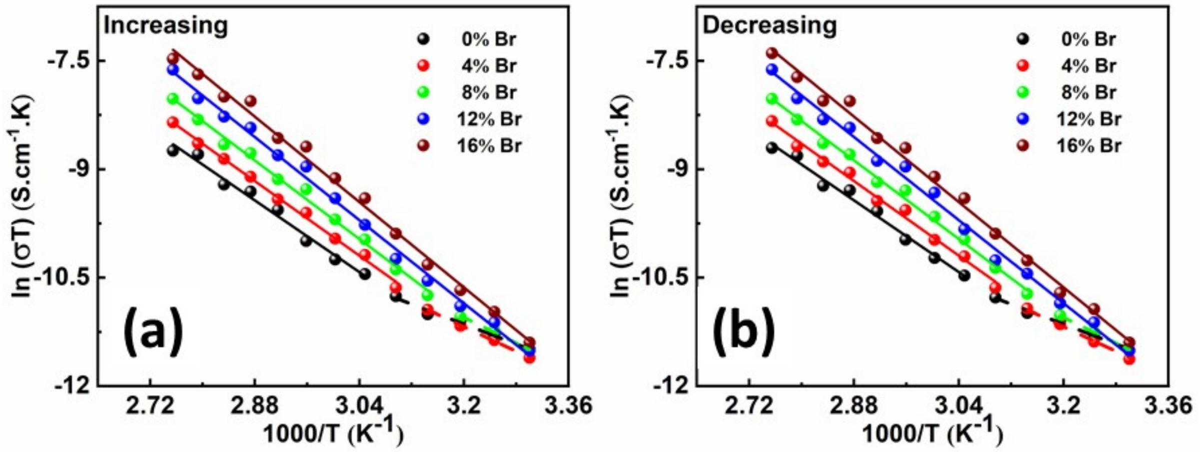

Fig. S8. The temperature-dependent conductivity of $MAPbI_3$ and $MAPb(Br_xI_{1-x})_3$ SCs. E_a is the activation energy of ions (Arrhenius plot).

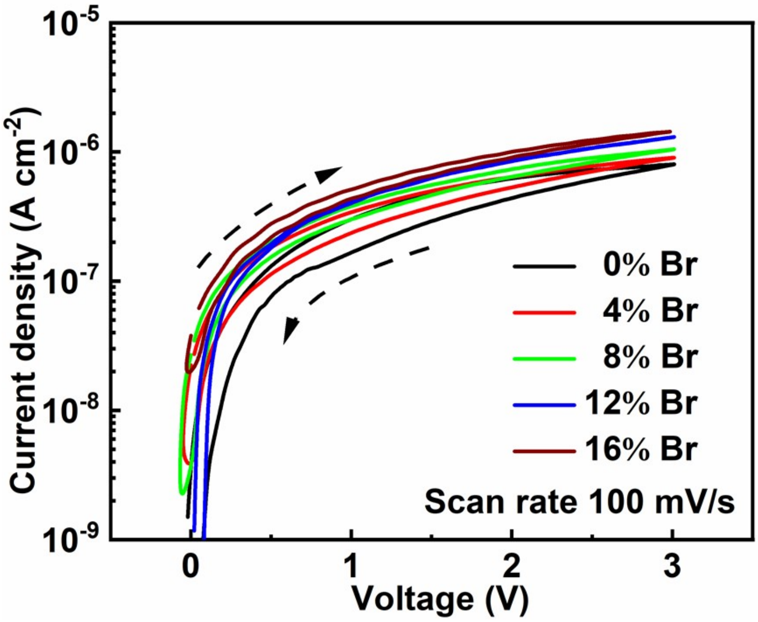

Fig. S9. I–V hysteresis plots of $MAPbI_3$ and $MAPb(I_{1-x}Br_x)_3$ SCs.

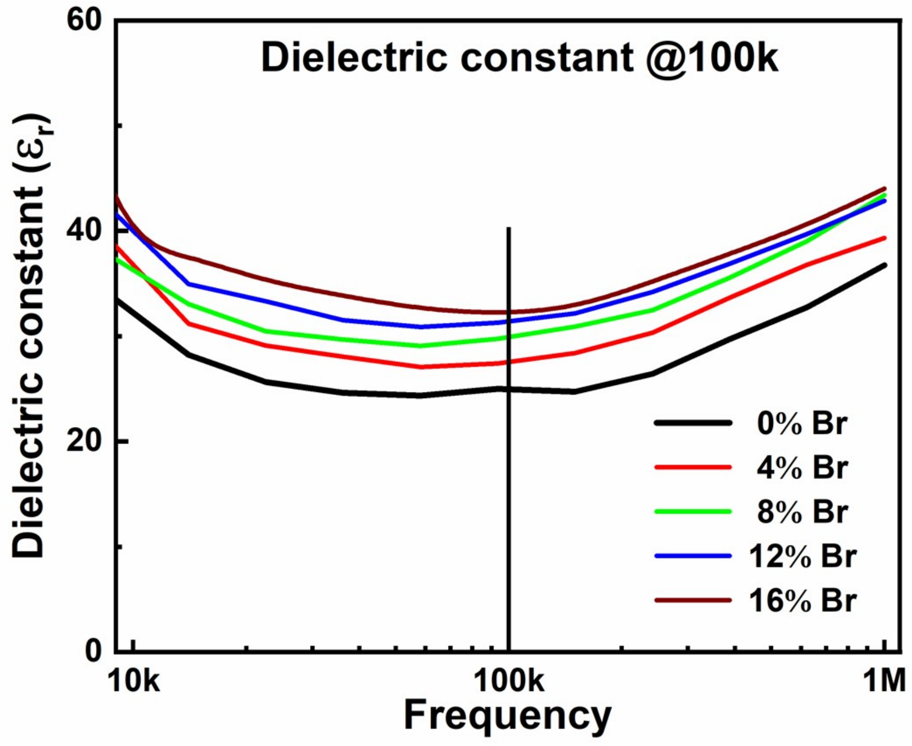

Fig. S10. Dielectric constant (ε_r) of $MAPbI_3$ and $MAPb(Br_xI_{1-x})_3$ SCs in the frequency range of 10 kHz to 1 MHz.

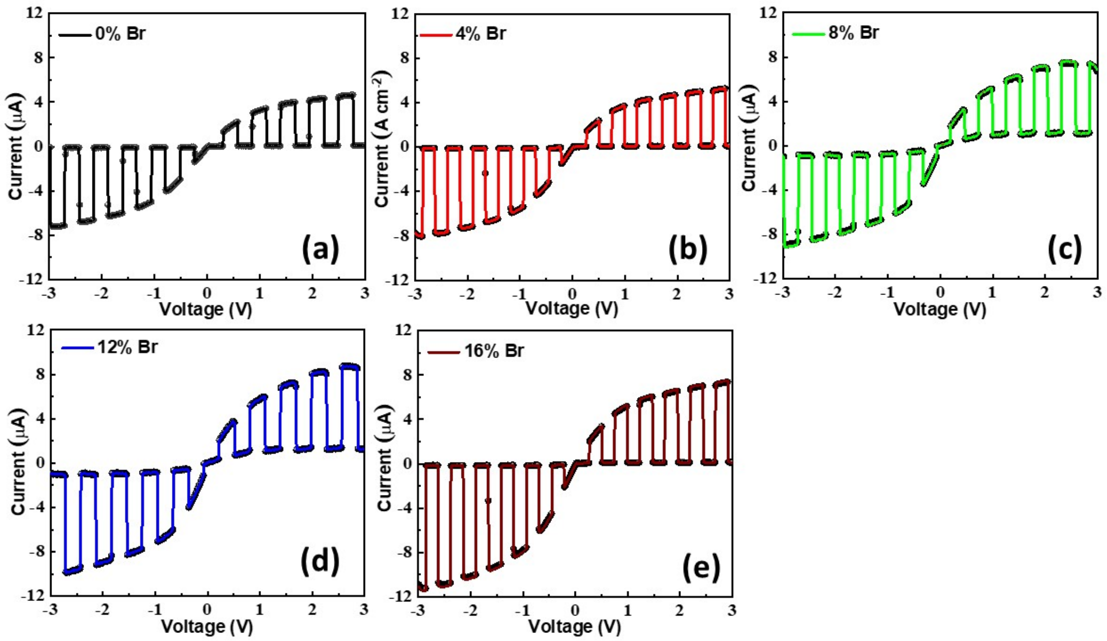

Fig. S11. Current-voltage curves of (a) $MAPbI_3$ and (b-e) $MAPb(Br_xI_{1-x})_3$ SCs based planar-type PDs.

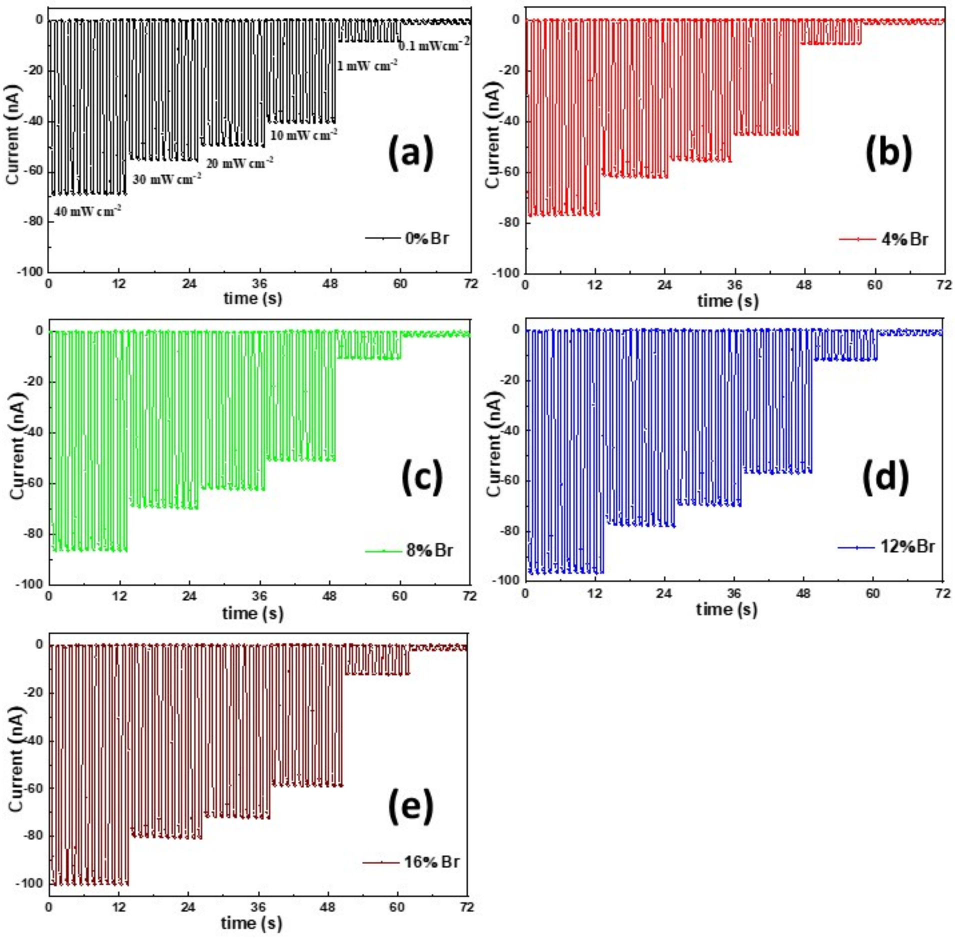

Fig. S12. Intensity-dependent photoresponse of (a) $MAPbI_3$ and (b-e) $MAPb(Br_xI_{1-x})_3$ SCs based planar-type PDs.

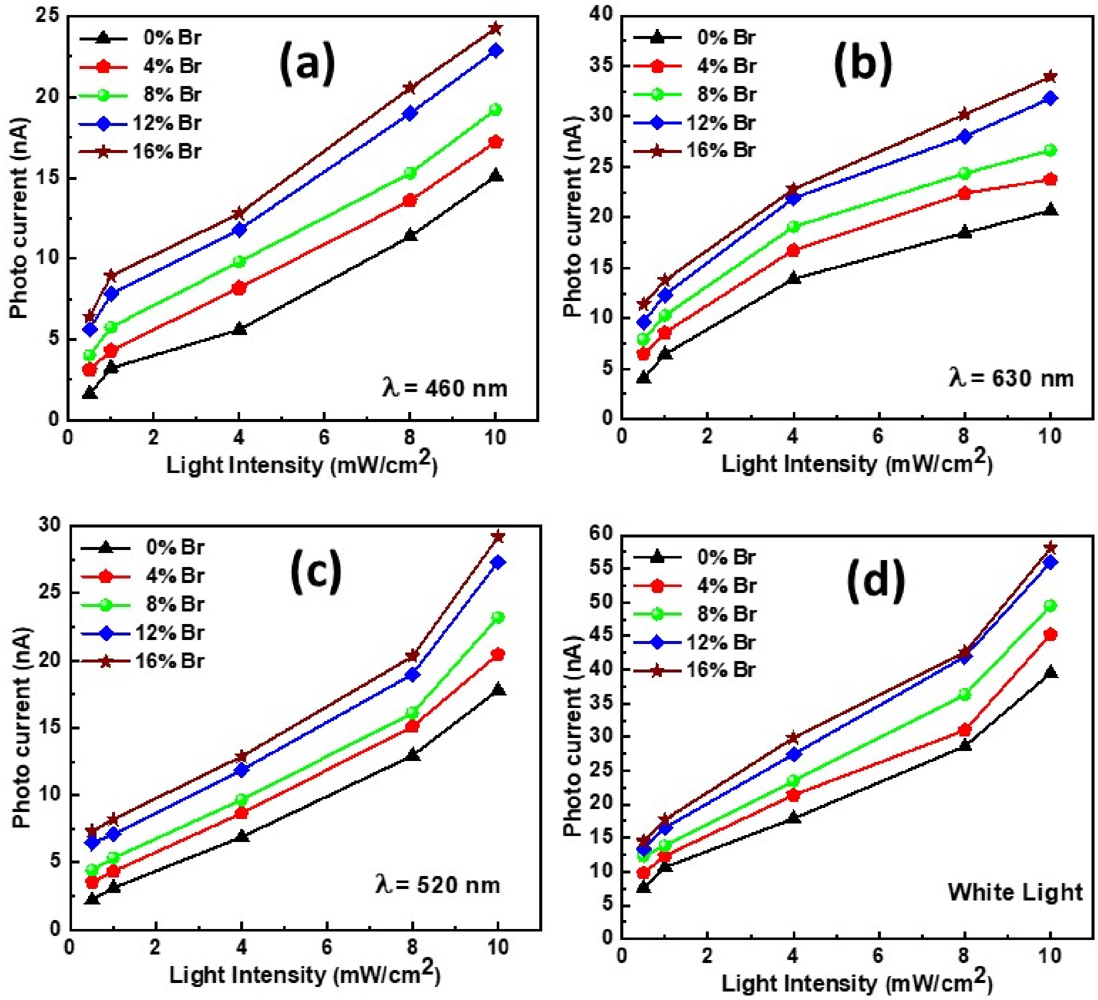

Fig. S13. Photocurents of $MAPbI_3$ and $MAPb(I_{1-x}Br_x)_3$ SC based planar PDs at different wavelengths as a function of light intensity.

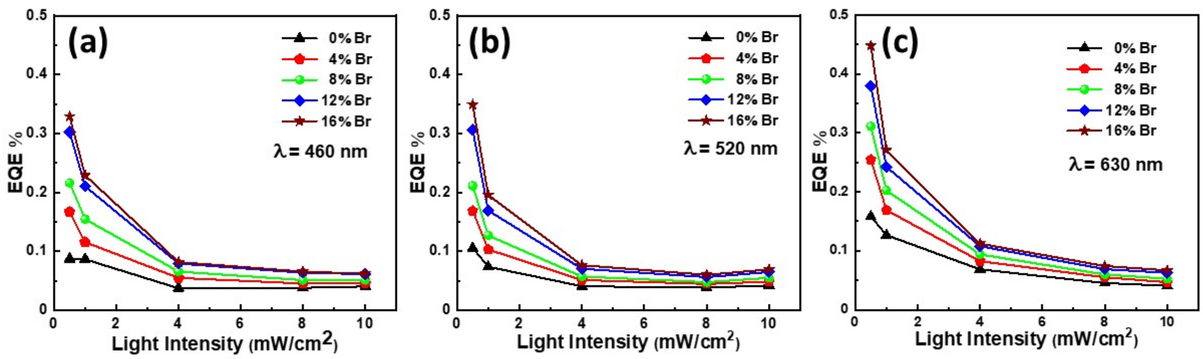

Fig. S14. External quantum efficiency (EQE) of $MAPbI_3$ and $MAPb(Br_xI_{1-x})_3$ SC based planar PDs at different wavelengths as a function of light intensity.

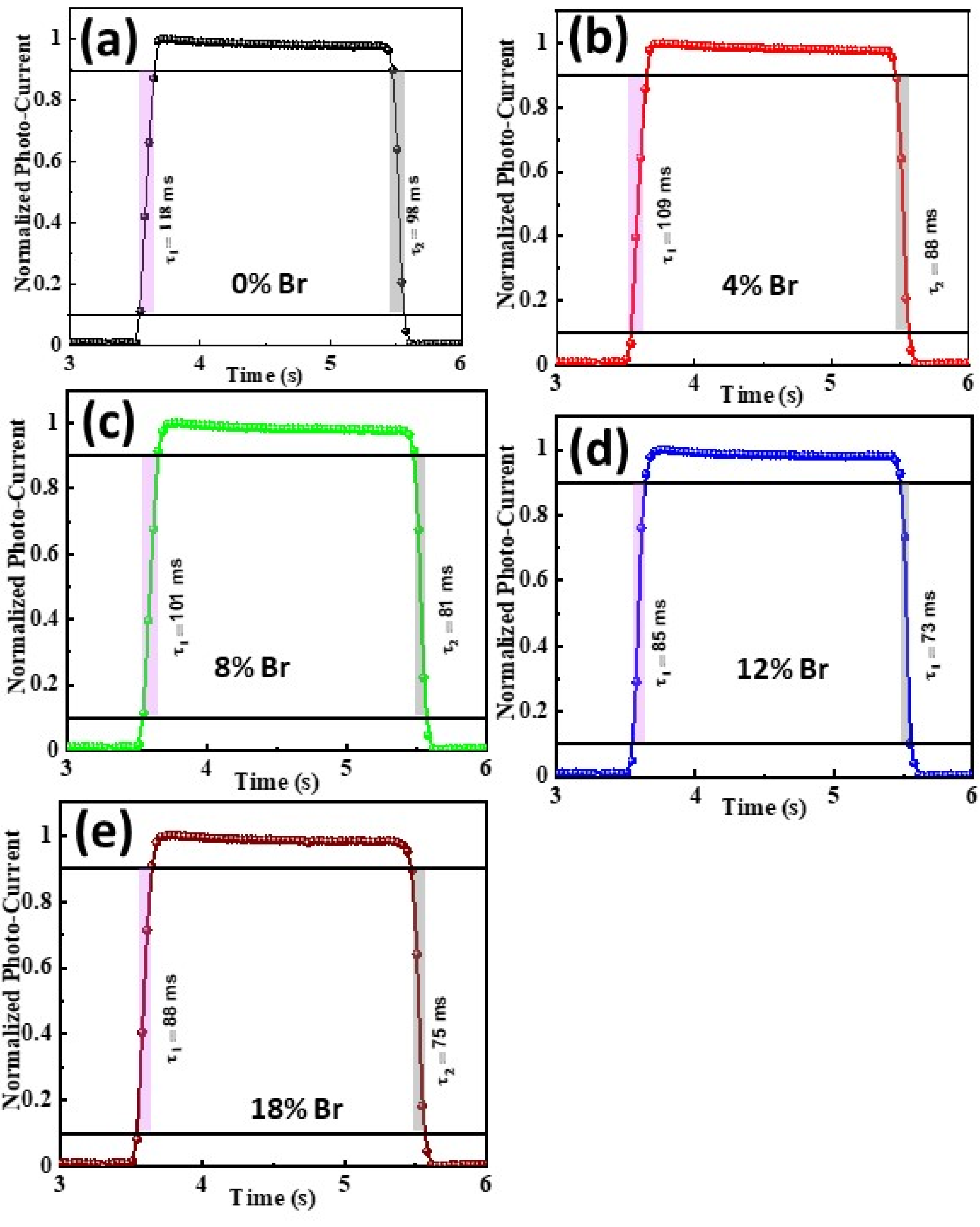

Fig. S15. Photocurents of $MAPbI_3$ and $MAPb(Br_xI_{1-x})_3$ SC based planar PDs at different wavelength as a function of light intensity.

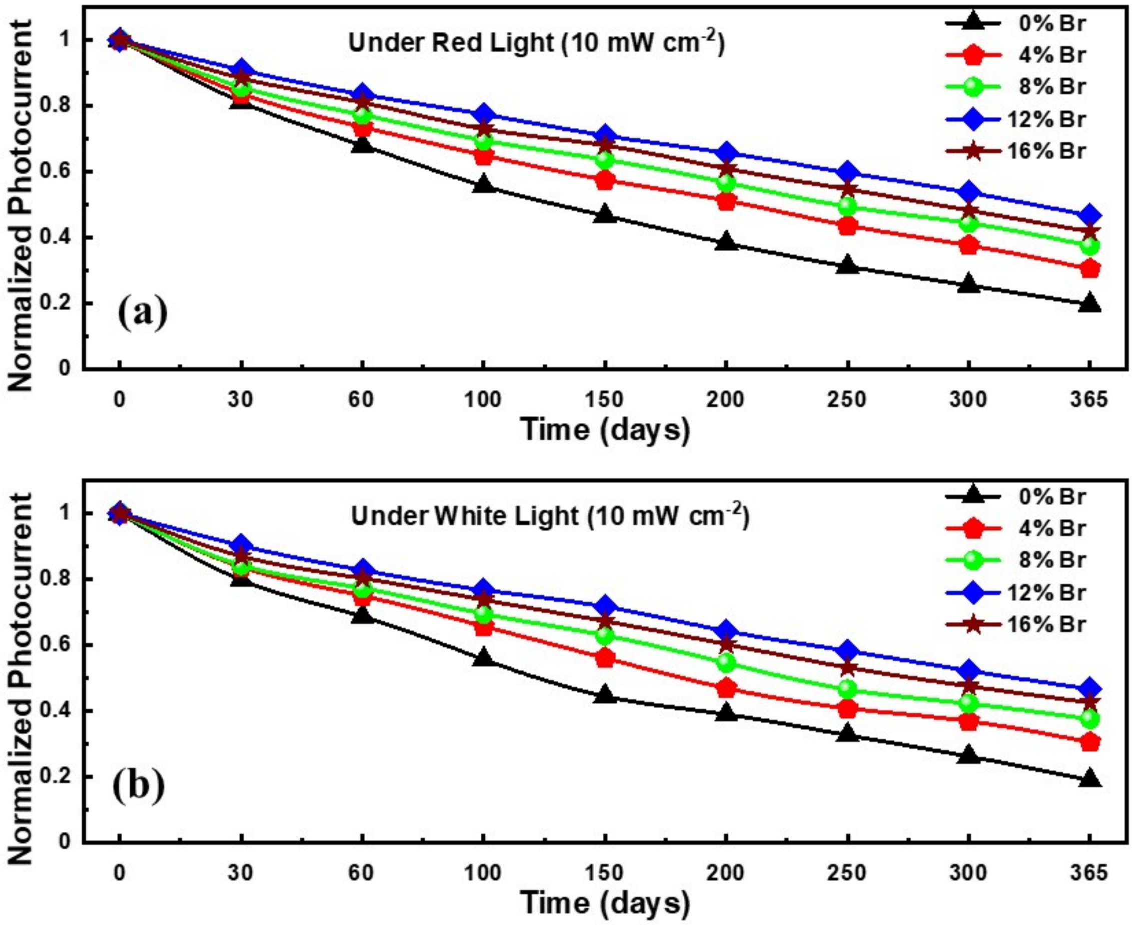

Fig. S16. Normalized photocurrent under (a) red light (630 nm) and (b) white light at 10 mW cm^{-2} as a function of time.

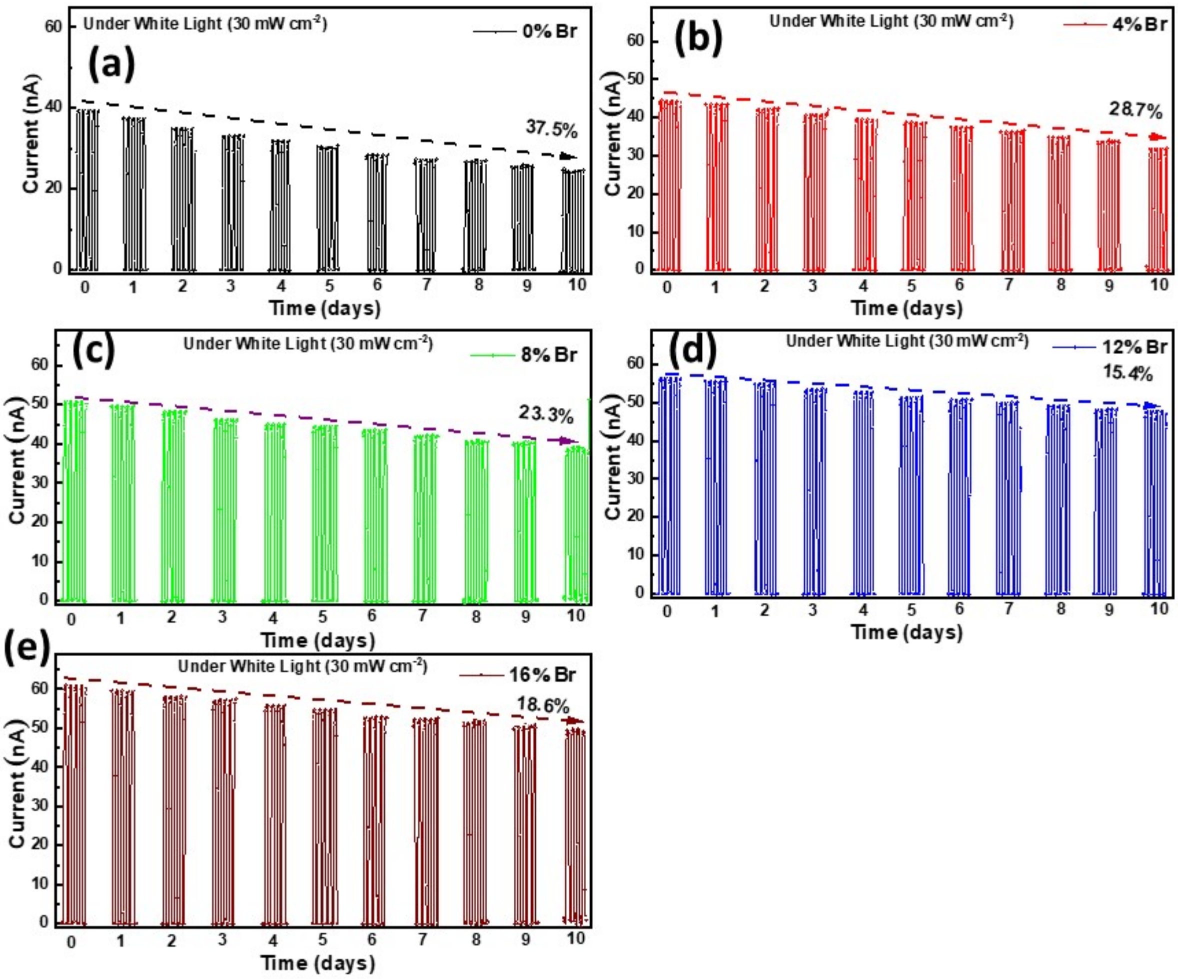

Fig. S17. Long term photocurrent of $MAPbI_3$ and $MAPb(Br_xI_{1-x})_3$ SC based planar PDs at different wavelength.

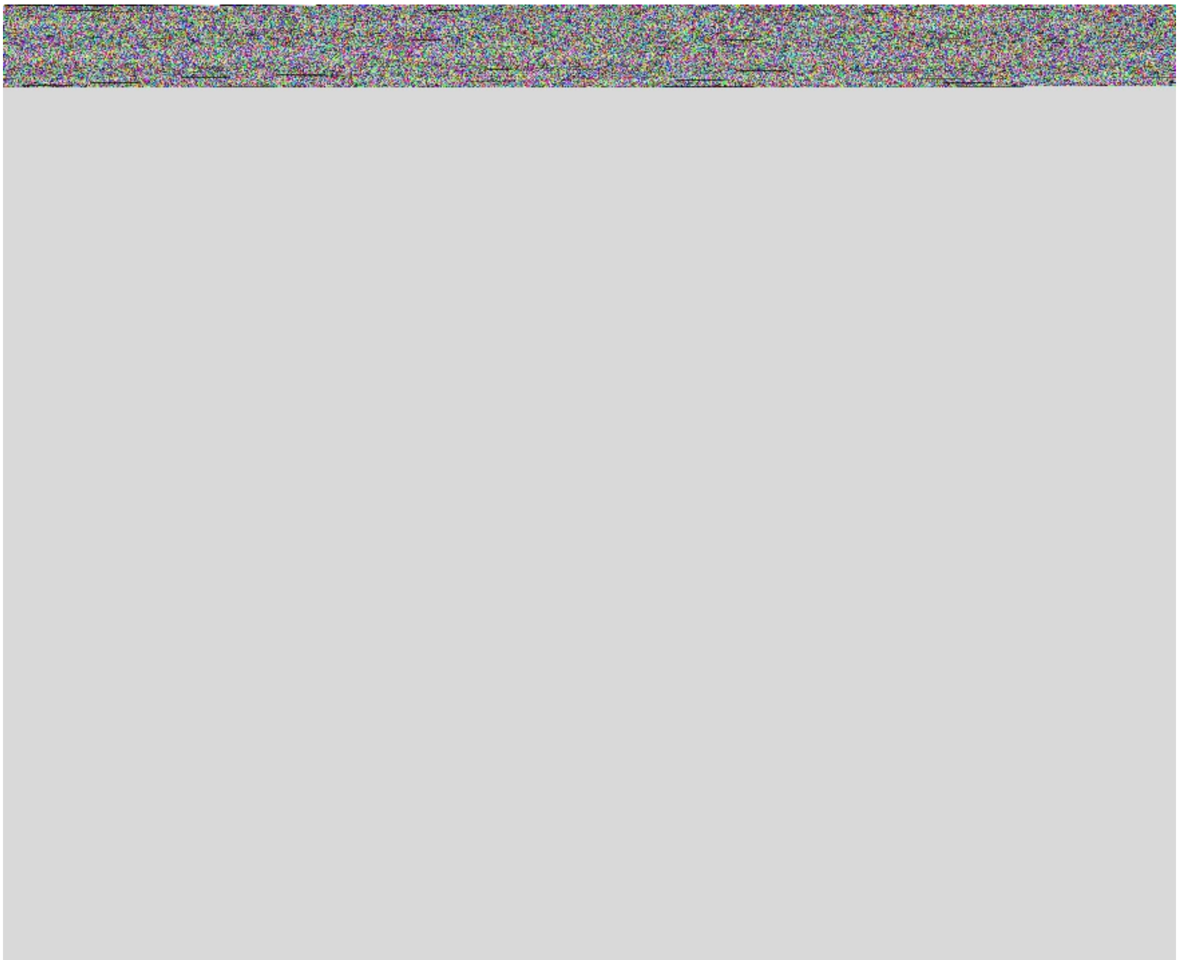

Fig. S18. Photoresponse of (a) $MAPbI_3$ and (b-e) $MAPb(Br_xI_{1-x})_3$ SCs based planar-type PDs under continuous operation.

Table S1. Halide percentage calculation incide crystals using EDX data.

Crystal Composition	Iodine (Atomic %)	Bromide (Atomic %)	Avarage Br percenrage (Atomic %)
$MAPb(Br_{0.04}I_{0.96})_3$	95.76	4.24	4.01%
	96.07	3.93	
	96.13	3.87	
$MAPb(Br_{0.08}I_{0.92})_3$	92.09	7.91	7.92%
	92.33	7.77	
	91.91	8.09	
$MAPb(Br_{0.12}I_{0.88})_3$	87.87	12.13	12.04%
	88.20	11.80	
	87.82	12.18	
$MAPb(Br_{0.16}I_{0.84})_3$	83.63	16.37	15.97%
	84.22	15.88	
	84.34	15.66	

Table S2. The calculated activation energies for $MAPbI_3$ and (b-e) $MAPb(Br_xI_{1-x})_3$ SCs.

Crystal Composition	From Conductivity				From EIS (decresing cycle)	
	Incresing cycle		Decresing cycle		E_a (cubic) (eV)	E_a (tetragonal) (eV)
	E_a (cubic) (eV)	E_a (tetragonal) (eV)	E_a (cubic) (eV)	E_a (tetragonal) (eV)		
$MAPbI_3$	0.52±0.012	0.35±0.011	0.53±0.007	0.34±0.012	0.52±0.008	0.34±0.007
$MAPb(Br_{0.04}I_{0.96})_3$	0.55±0.013	0.36±0.012	0.55±0.013	0.34±0.013	0.54±0.013	0.35±0.020
$MAPb(Br_{0.08}I_{0.92})_3$	0.58±0.016	0.37±0.018	0.57±0.010	0.38±0.016	0.57±0.009	0.39±0.038
$MAPb(Br_{0.12}I_{0.88})_3$	0.62±0.011	*	0.62±0.011	*	0.59±0.011	*
$MAPb(Br_{0.16}I_{0.84})_3$	0.61±0.015	*	0.61±0.015	*	0.59±0.012	*